Journal of Solid State Chemistry **159,** 113–120 (2001)
doi:10.1006/jssc.2001.9138, available online at http://www.idealibrary.com on IDEAL®

Structure and Thermal Stability of the New Intermetallics $MgPd_2$, $MgPd_3$, and Mg_3Pd_5 and the Kinetics of the Iodine-Catalyzed Formation of $MgPd_2$

Ch. Wannek and B. Harbrecht[1]

Department of Chemistry and Materials Science Centre, Philipps University of Marburg, Hans-Meerwein-Straße, D-35032 Marburg, Germany

Received November 2, 2000; in revised form February 14, 2001; accepted March 5, 2001; published online May 11, 2001

Three new binary intermetallics in the palladium-rich part of the magnesium–palladium system have been identified and characterized by combining preparative methodologies with powder X-ray diffraction techniques and thermochemical analyses. $MgPd_2$ decomposing in the solid state at 628(2)°C adopts a Co_2Si-type structure: space group *Pnma*, $a = 5.4421(2)$, $b = 4.1673(2)$, $c = 8.0129(3)$ Å. $MgPd_3$ crystallizes in a Al_3Zr-type structure: space group *I4/mmm*, $a = 3.92263(7)$, $c = 15.6527(4)$ Å. It decomposes in a peritectoid reaction at 704(2)°C. The kinetics of the iodine-catalyzed synthesis of $MgPd_2$ have been studied. The reactions seem to follow Ostwald's step rule. Four intermediate phases were identified, among them was Mg_3Pd_5, a previously unknown phase with a Ge_3Rh_5-type structure: space group *Pbam*, $a = 5.427(2)$, $b = 10.588(5)$, $c = 4.1304(12)$ Å.

INTRODUCTION

Strong heteroatomic interactions are the reason why many intermetallic systems consisting of a valence-electron-rich transition metal and an electropositive element form alloys of extraordinary stability (1–3). Enthalpy as a driving force favors the formation of a substantial number of distinct intermetallic phases, resulting in relatively complex phase diagrams (4). The clean solid state synthesis of such phases exclusively forming in the solid state is often found to be heavily impeded or impossible, even at their upper limit of stability. This is particularly true if the phase already decomposes some hundred degrees below the lowest eutectic adjacent to the peritectoid temperature. In this case, a catalytically stimulated reaction between the metal components may help to overcome the sluggish diffusion of the atoms in the solid thus providing access to new ordered intermetallics. Previous studies of the Al–Pd (5), Al–Pt (6), and Ga–Pd systems (7) have shown that such diffusion barriers may be overcome by adding catalytically effective amounts of iodine to the reaction mixture. In the present study we apply this particular preparative methodology in search of new Mg–Pd binaries.

In the Mg–Pd system, two phases near 50 at.% Pd have been reported: MgPd with CsCl-type structure (8) and $Mg_{0.9}Pd_{1.1}$ adopting the AuCu structure (9); it was concluded (10) that Mg_2Pd_3 (11) is identical with $Mg_{0.9}Pd_{1.1}$. No intermediate phase richer in palladium has been characterized yet, but when f.c.c. solid solutions near the composition $Mg_{25}Pd_{75}$ were annealed at 500°C, additional lines in X-ray photographs were observed indicating the formation of an ordered intermetallic compound. The reflections were tentatively indexed on the basis of a cubic unit cell with $a = 3.920$ Å (8).

As a result of a systematic reinvestigation of the palladium-rich part of this system we have detected and characterized three new binary phases and briefly discuss their structural chemistry. Moreover, we give a first insight into the kinetics of their iodine-catalyzed formation, as seven equal reaction mixtures with the molar ratio Mg:Pd amounting 1:2 were quenched after different reaction times and analyzed quantitatively by Rietveld refinements of powder X-ray diffractograms.

EXPERIMENTAL

Synthesis

All samples were prepared on a 200–300 mg scale by reactions of appropriate amounts of the pure elements used as purchased (Pd: powder, 99.9%, Degussa; Mg: powder, 99.8%, Alfa) and catalytically effective amounts of iodine (< 0.05 equivalents, 99.5%, Merck) in evacuated fused-silica tubes (6 cm in length, 8 mm in diameter). The ampoules were heated with a rate of 50 K h^{-1} up to 600°C, maintained at this temperature for 48 h and subsequently

[1]To whom correspondence should be addressed.

0022-4596/01 $35.00

quenched in water. In the case of the experiments concerning the kinetics of the reaction, we have prepared seven ampoules of practically the same size loaded with Mg and Pd powders in molar ratios 1:2 and an overall mass of about 200 mg together with two small crystals of iodine (2–3 mg). All seven samples were put together into the same furnace, heated up to 600°C with a rate of 50 K h^{-1}, kept at this temperature and removed after different times. All products were washed with half-saturated aqueous KI solution to dissolve traces of iodine. The alloys were obtained as homogeneous grey powders showing no reactivity toward air and water. Within the resolution of the method, EDX analyses (CamScan CS 4DV, Noran Instruments) confirmed the absence of impurities heavier than boron. To perform annealing experiments, the alloys were filled in small corundum tubes, which in turn were put into silica tubes. These were evacuated and fused hereafter. The ampoules were placed in tube furnaces and heated to the appropriate temperatures for 3 days and subsequently quenched in water.

X-Ray Diffraction and Rietveld Analyses

All products were characterized by X-ray powder diffraction at room temperature. Photographs obtained by the Guinier technique (Huber Guinier system 600, Cu$K\alpha_1$ radiation, Si added as an internal standard (12)) were used to identify the phases present and for the refinements of lattice parameters with the local program DIFFRAKT (13). X-ray powder diffractograms of selected samples were recorded on a Philips X'Pert MPD or a Philips PW 1050/25 diffractometer, both operating in Bragg–Brentano geometry. The data were processed with the Philips X"Pert Plus (14) software. For the Rietveld refinements (15) of single-phase samples, the background was fitted by a polynomial (5 parameters) and the peak shape was described by a pseudo-Voigt function. All parameters (histogram scale factor, zero-point error, half-width parameters U, V, and W, lattice parameters, positional and independent thermal parameters for each atom) were refined simultaneously and independently in the last cycles of the refinements. As no significant indications for mixed occupancies or vacancies were detected when the occupation factors for all sites were refined, these were constrained to be equal to unity. In the case of the multiphase samples obtained within the kinetic studies, short-time diffractograms were collected ($15° \leq 2\Theta \leq 70°$, step size 0.03°, 3 s per step). In the course of the corresponding Rietveld calculations, only the background, the zero-point error, all scale factors, and all lattice parameters were refined. The structural parameters were fixed, the half-width parameters were only refined for the main product. Phases calculated to be present with less than 2 weight% were omitted in the following cycles. More details will be given in the corresponding paragraph.

Physical Measurements

Thermochemical analyses were performed with a DSC system (Setaram setsys 16/18) using pressed powder pellets (19.7 to 79.3 mg) placed in corundum crucibles. The samples were heated with a rate of 10 K min^{-1} in a purified argon atmosphere. The results given are the mean values for at least two measurements of independent samples. The values were taken from the second heating cycles respectively, estimated standard deviations amount to less than 3 K. The calibration of the temperature was performed using Al and Ag standards. Conductivity measurements were performed between 12 and 300 K on bars sintered at 600°C using a DC four-terminal method. Electrical contacts to the bar were made with silver paint.

RESULTS AND DISCUSSION

$MgPd_2$

All reflections on Guinier photographs of $MgPd_2$ could be indexed on the basis of an orthorhombic unit cell. The reflection conditions observed were compatible with the space group *Pnma*. Assuming this symmetry, the crystal structure was solved from the intensities of an X-ray powder diffractogram by means of direct methods with help of the SHELXS-86 software (16) and refined by a Rietveld profile fit (Fig. 1, Table 1).

$MgPd_2$ has a Co_2Si-type structure (Table 2), which is a special branch of the (anti-)$PbCl_2$-type having hundreds of representatives among binary or ternary intermetallics (17). In the Co_2Si-type of AB_2 structures, the atoms of the minor component are 10-fold coordinated in the form of AB_6 prisms whose rectangular faces are capped by four additional B atoms in the same plane. The linking and mutual orientation of these prisms, resulting in puckered layers

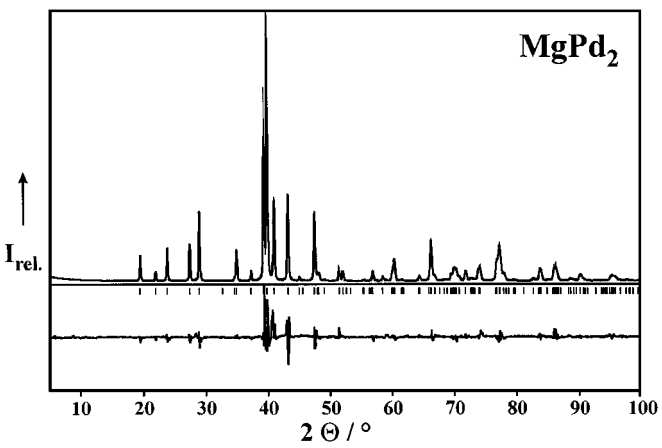

FIG. 1. Observed and calculated powder diffraction profiles of (top), $MgPd_2$, (scale 1.5:1, bottom) the difference plot of the Rietveld refinement, and (middle) the reflection positions.

TABLE 1
Additional Details for the Rietveld Refinements for $MgPd_2$ and $MgPd_3$

	$MgPd_2$	$MgPd_3$
Data collection parameters		
Diffractometer type	Philips PW 1050/25	Philips X'Pert-MPD
Radiation	Cu$K\alpha$	Cu$K\alpha$
Temperature	RT	RT
Angular range (°)	$5.00 \le 2\Theta \le 100.00$	$5.01 \le 2\Theta \le 99.99$
Step size (°)	0.025	0.020
Scan mode	stepwise	continuous
Collection time per interval (s)	20	25
Solution and refinement of the crystal structure		
Program for the processing of the original data	DIFFRAKT (13)	DIFFRAKT (13)
Program for the solution of the structure	SHELXS-86 (16)	SHELXS-86 (16)
Program for the Rietveld refinement	X'Pert Plus (14)	X'Pert Plus (14)
Number of reflections	111	55
Number of refined parameters	24	20
Number of structural parameters	9	5
R_P	0.093	0.072
wR_P	0.128	0.103
R_B	0.042	0.048

Note. $R_P = \sum|y_{io} - y_{ic}|/\sum \quad y_{io}$; $wR_P = [\sum w_i(y_{io}-y_{ic})^2/\sum w_i y_{io}^2]^{1/2}$; $R_B = \sum|I_{ko} - I_{kc}|/\sum I_{ko}$ where y_{io} and y_{ic} are the observed and calculated countrates at the ith step, respectively, w_i is a weighting factor, based on counting statistics (14), and I_o and I_c are the observed and calculated intensities for all allowed reflections.

being shifted about half a lattice parameter b with respect to the neighboring layers, is visualized in Fig. 2. For the atoms of the major component C.N. 13 is realized (Table 3). From a topological point of view this structure represents an intermediate arrangement between the hexagonal $InNi_2$-type of structure and the face-centered cubic Cu-type (18). The relationship of the (anti)-$PbCl_2$-type or TiNiSi-type structure (space group *Pnma*) to the $CeCu_2$ type of higher symmetry (space group *Imma*) has been pointed out, although the features of structure and bonding are significantly different in the Co_2Si subgroup of structures (19).

TABLE 2
Structural Parameters of $MgPd_2$

Atom	Site	x	y	z	B_{iso} (10^4 pm^2)
Mg	4c	0.327(2)	$\frac{1}{4}$	0.1025(9)	0.7(2)
Pd(1)	4c	0.3370(4)	$\frac{1}{4}$	0.4285(3)	1.54(5)
Pd(2)	4c	0.4398(4)	$\frac{1}{4}$	0.7659(2)	1.64(6)

Note. Space group *Pnma*, $a = 5.4421(2)$ Å, $b = 4.1673(2)$ Å, $c = 8.0129(3)$ Å.

At 628°C $MgPd_2$ decomposes in a peritectoid reaction into a mixture of $MgPd_3$ (see next paragraph; $a = 3.940(11)$, $c = 15.643(9)$ Å) and MgPd ($a = 3.122(5)$ Å), the latter being remarkable as according to the published phase diagram $Mg_{0.9}Pd_{1.1}$ was expected to form instead. The Co_2Si- type structure with palladium as major component had been found to exist in seven binary systems (4). It is formed with all elements of group 13 (except for boron), with magnesium, zinc, and tin. The fact that it occurs with aluminium and all its heavier homologues although the atomic volumes of thallium and aluminium differ by a factor of 1.73 (20), indicates that electronic effects must play the most important role in determining the type of crystal structure formed in these systems. In this context it is noteworthy that the volume fraction of the Dirichlet domains (DIDO95 (21)) of the minor component atoms standardized to the volume of the unit cell is independent of the size differences between the two components: it just varies between 32.2% for $GaPd_2$ and 33.0% for $MgPd_2$.

$MgPd_3$

Extensive heat treatments of f.c.c. solid solutions near the composition $Mg_{25}Pd_{75}$ at 500°C indicated the existence of an ordered compound $MgPd_3$. Additional lines on X-ray powder photographs were tentatively indexed assuming a cubic lattice with $a = 3.920$ Å (12). We directly prepared this compound at 600°C and were able to index all reflections on Guinier photographs on the basis of a tetragonal body-centered unit cell, according to the intensity modulations obviously representing a 4c superstructure of f.c.c. Pd. In accordance with the reflection conditions observed, we solved the crystal structure in space group *I*4/*mmm* from the intensities of an X-ray diffractogram and refined it by a Rietveld profile fit (Fig. 3, Table 1). As $MgPd_3$ coexists with the neighboring Mg_xPd_{1-x} solid solution, we performed the Rietveld calculations in and excluding the reflections of the cubic subcell. Both refinements led to the same results within the standard deviations of the values obtained.

$MgPd_3$ has the Al_3Zr-type structure (Tables 3 and 4), which is a member of a class of superstructures derived from the cubic $AuCu_3$ type by introducing antiphase boundaries with a displacement vector of $1/2\ \langle 1\,1\,0\rangle$ parallel to the (0 0 1) plane after different numbers of cubic subcells. The simplest representative of this type of structures is Al_3Ti (Pearson symbol tI8) having a stacking sequence **AB** of atomic double-layers. In the Al_3Zr structure, planes are shifted only after every second subcell, resulting in an **AABB** or $\mathbf{A^2B^2}$ sequence. Alloys with smaller frequencies of "stacking faults" as for example $\mathbf{A^3B^3}$ in $PbPd_9Tl_2$ (22) or even $\mathbf{A^9B^9}$ in $Cu_{3+x}Pd_{1-x}$ (23) have been found; the $AuCu_3$ structure can be regarded as the end member with $\mathbf{A}^\infty\mathbf{B}^\infty$ (Fig. 4; crystallographic cell edges omitted for clarity). In all

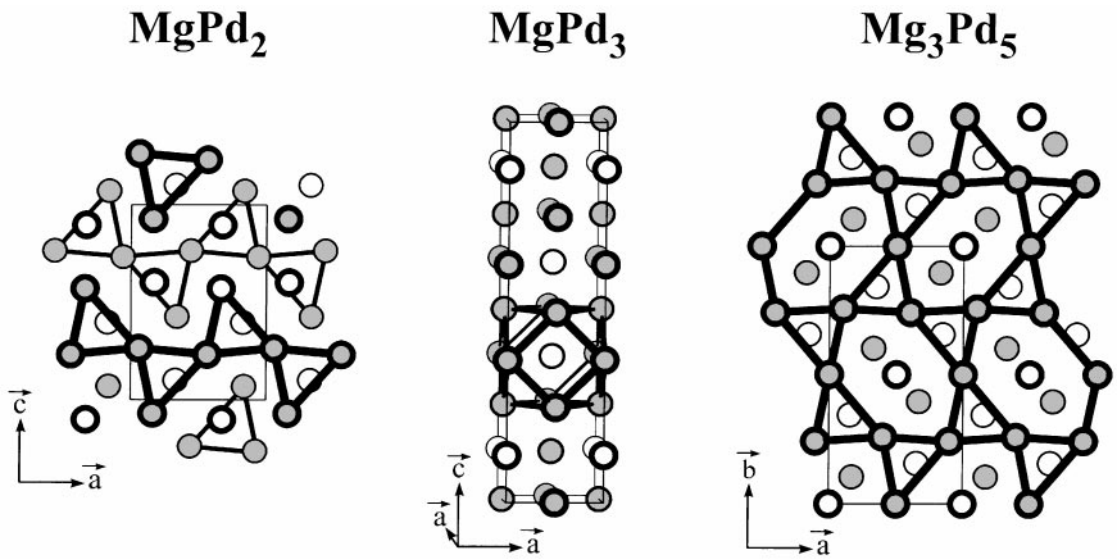

FIG. 2. The crystal structures of $MgPd_2$, $MgPd_3$, and Mg_3Pd_5. White circles represent Mg atoms, grey circles represent Pd atoms. Atoms shown as bold circles are located nearer to the viewer than the others.

these structures the coordination of the atoms in the first sphere is essentially the same.

Ab initio calculations have been carried out concerning the competition of the simplest structure types for a chemical composition given; for a review see Ref. (24). The deeper understanding of the mechanism of the stabilization of structures with long period stacking remains a fascinating challenge.

Thermoanalytical measurements on $MgPd_3$ showed an endothermic effect at 704°C. Annealing experiments verified the phase to decompose in a peritectoid reaction above 700°C into a mixture of Mg_xPd_{1-x} ($a = 3.9190(2)$ Å) and CsCl-type MgPd ($a = 3.1191(2)$ Å). No indications for the existence of other tetragonal superstructures at different temperatures or compositions were found.

Mg_3Pd_5 and the Kinetics of the Formation of $MgPd_2$

While the thermodynamic aspects of chemical transport reactions become increasingly better understood (25–27), less is known about the mechanism and the kinetics of the iodine-catalyzed formation of the intermetallics discussed here (28–31). We focus on a kinetic aspect of this iodine-catalyzed reaction without spatial transport. We performed

TABLE 3
Interatomic Distances (< 4 Å) for $MgPd_2$

Mg–Pd(1)	2.613(7) × 1	–Pd(2)	2.871(2) × 2
–Pd(2)	2.658(5) × 2	–Pd(2)	2.882(2) × 2
–Pd(1)	2.662(5) × 2	–Pd(1)	2.967(2) × 2
–Pd(1)	2.679(9) × 1	–Pd(2)	3.267(3) × 1
–Pd(2)	2.766(7) × 1	–Pd(1)	3.948(3) × 2
–Pd(1)	2.786(9) × 1		
–Pd(2)	2.858(6) × 2	Pd(2)–Mg	2.658(5) × 2
–Mg	3.253(9) × 2	–Pd(2)	2.733(3) × 2
–Mg	3.604(11) × 2	–Pd(1)	2.761(3) × 1
–Pd(2)	3.627(8) × 1	–Mg	2.766(7) × 1
		–Mg	2.858(6) × 2
Pd(1)–Mg	2.613(7) × 1	–Pd(1)	2.871(2) × 2
–Mg	2.662(5) × 2	–Pd(1)	2.882(2) × 2
–Mg	2.679(9) × 1	–Pd(1)	3.267(3) × 1
–Pd(2)	2.761(3) × 1	–Mg	3.627(8) × 1
–Mg	2.786(9) × 1		

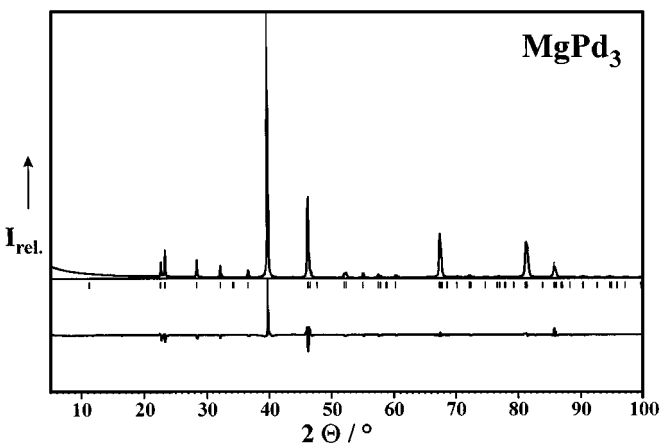

FIG. 3. Observed and calculated powder diffraction profiles of (top) $MgPd_3$, (scale 1.5:1, bottom) the difference plot of the Rietveld refinement, and (middle) the reflection positions.

TABLE 4
Structural Parameters of $MgPd_3$

Atom	Site	x	y	z	B_{iso} (10^4 pm^2)
Mg	4*e*	0	0	0.1242(10)	0.5[a]
Pd(1)	4*c*	0	$\frac{1}{2}$	0	0.84(6)
Pd(2)	4*d*	0	$\frac{1}{2}$	$\frac{1}{4}$	1.57(6)
Pd(3)	4*e*	0	0	0.3742(2)	1.19(3)

Note. Space group $I4/mmm$, $a = 3.92263(7)$ Å, $c = 15.6527(4)$ Å.
[a]Not refined.

TABLE 5
Interatomic Distances (< 4 Å) for $MgPd_3$

Mg–Pd(1)	$2.762(11) \times 4$	Pd(2)–Pd(3)	$2.761(3) \times 4$
–Pd(3)	$2.7738(2) \times 4$	–Pd(2)	$2.77372(3) \times 4$
–Pd(2)	$2.779(11) \times 4$	–Mg	$2.779(11) \times 4$
–Mg	$3.89(2) \times 1$	–Pd(1)	$3.91318(10) \times 2$
–Pd(3)	$3.91(2) \times 1$	–Pd(2)	$3.92263(7) \times 4$
–Mg	$3.92263(7) \times 4$		
		Pd(3)–Pd(2)	$2.761(3) \times 4$
Pd(1)–Mg	$2.762(11) \times 4$	–Mg	$2.7738(2) \times 4$
–Pd(1)	$2.77372(3) \times 4$	–Pd(1)	$2.780(3) \times 4$
–Pd(3)	$2.780(3) \times 4$	–Mg	$3.91(2) \times 1$
–Pd(2)	$3.91318(10) \times 2$	–Pd(3)	$3.92263(7) \times 4$
–Pd(1)	$3.92263(7) \times 4$	–Pd(3)	$3.940(5) \times 1$

seven similar experiments to study the reaction pathway of the formation of $MgPd_2$ as described in detail in the Experimental section. The reactions were aborted after different times by quenching. Rietveld refinements of powder diffractograms of all samples enabled us to calculate the amounts of phases present at the various reaction stages. The standard deviations of the atomic fractions of the respective phases were calculated (14) to amount 0.3–0.9%, though the values in Table 6 are given in full percents. In all cases, the refinements could be carried out without any difficulties, especially all reflections observed could be indexed (e.g., in the 2 h sample, Fig. 5). As the (1 1 0) reflection of CsCl-type MgPd carried much more intensity than expected, the region between $40.5^\circ \leq 2\Theta \leq 41.5^\circ$ was excluded during the refinements for samples containing this phase. From the results summarized in Table 6, the following conclusions can be drawn.

(i) The reaction is very fast and obviously starts at temperatures lower than 600°C. In the sample immediately taken when this temperature was reached after heating from RT with a rate of 50 K h^{-1} no Mg and only 23% Pd could be

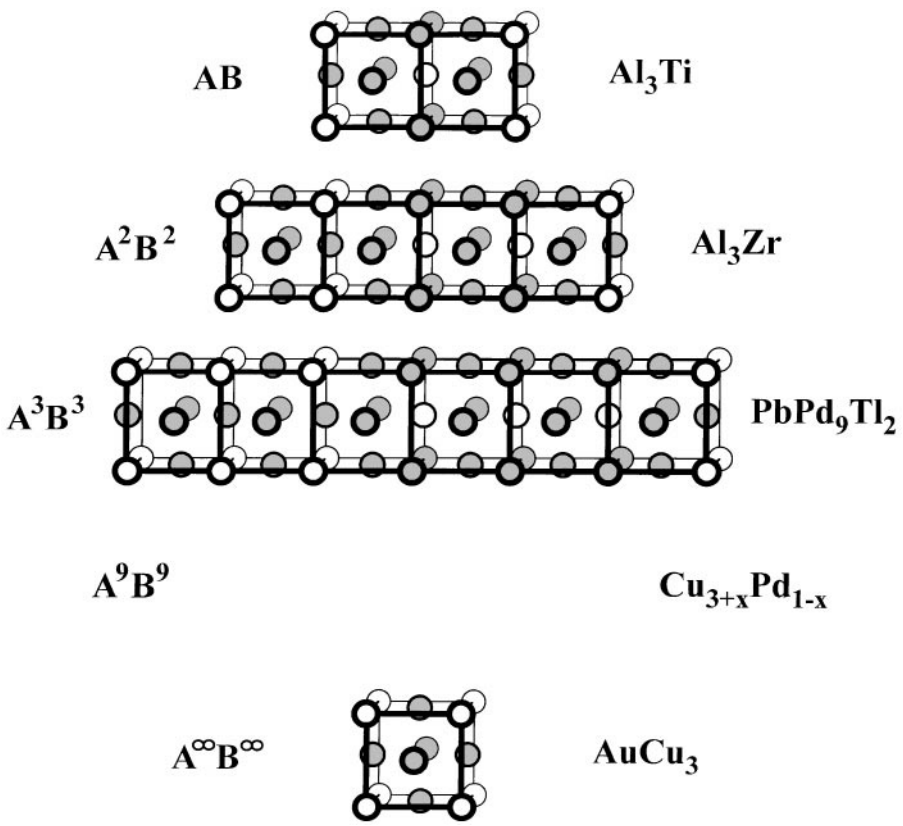

FIG. 4. Various superstructures of the $AuCu_3$ type with tetragonal symmetry.

TABLE 6
Kinetics of the Formation of $MgPd_2$—Amounts of Phases Present as Refined (Atomic Percent)

Time[a]	$Mg_{0.9}Pd_{1.1}$ (AuCu)[b]	MgPd (CsCl)	Mg_3Pd_5	$MgPd_2$	$MgPd_3$	Pd	Refined compositon
0 h	18	39	—	—	20	23	$MgPd_{1.99}$
2 h	—	37	—	20	34	9	$MgPd_{1.97}$
4 h	—	22	—	38	40	—	$MgPd_{1.97}$
7 h	—	13	—	65	22	—	$MgPd_{1.97}$
10 h	—	—	17	72	11	—	$MgPd_{2.02}$
13 h	—	—	11	82	7	—	$MgPd_{2.01}$
48 h	—	—	—	100	—	—	$MgPd_{2.00}$

[a]Time was set to $t = 0$ h when the temperature of 600°C was reached after the heating process.

[b]Refined as MgPd with atomic ratios 1:1.

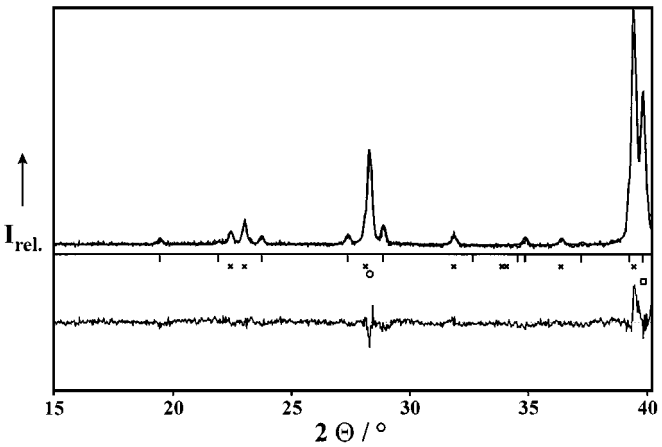

FIG. 5. Detail of the four-phase Rietveld refinement of the 2-h sample. The Bragg positions of the reflections are marked. Top to bottom: (bars) $MgPd_2$, (crosses) $MgPd_3$, (circle) MgPd, (square) Pd.

found. The largest parts of the starting elements had already been consumed for the formation of binary phases. The lattice parameter of the f.c.c. phase ($a = 3.8892(7)$ Å) identifies it to be pure Pd.

(ii) In the early stages of the reaction, a nonequilibrium mixture of phases is formed. No $MgPd_2$ could be detected in the first sample. The reaction proceeds via metastable phase mixtures. It seems to follow Ostwald's step rule with different intermediate phases appearing, gaining temporarily in weight fraction, and disappearing again.

(iii) First found in the 2 h sample, the atomic fraction of $MgPd_2$ on the whole sample steadily increases with time. After 48 h, the powder diffractogram exclusively shows the sharp reflections of Co_2Si-type $MgPd_2$ (Fig. 2). The lattice parameters refined for all samples remain unchanged in time within their estimated standard deviations.

(iv) One of the intermediate phases was identified to be the previously unknown Mg_3Pd_5. Fifteen reflections unambiguously arising from this phase could be conclusively indexed assuming an orthorhombic lattice with the parameters $a = 5.427(2)$, $b = 10.588(5)$, and $c = 4.1304(12)$ Å. The analysis of the lattice parameters, reflection conditions, and intensity modulations enabled us to assign it to the Ge_3Rh_5 structure type, space group *Pbam*, Fig. 2; bonding Pd–Pd interactions in one of the two crystallographic distinct planes perpendicular to the *b* axis is emphasized. This structure type is known to have 10 representatives (4). The result of the three-phase Rietveld refinement (10 h sample, Table 6) is shown in Fig. 6. The positional parameters of Mg_3Pd_5 were taken from Ga_3Pd_5 (4). Mg_3Pd_5 is the first example containing an element from the second main group as a minor component, all other phases are formed with an element from the third or fourth main group or the transition metals Ti and Hf while a valence-electron-rich transition metal (Ru, Rh, Pd, or Pt) serves as a major component. Since we did not succeed in preparing single-phase samples of Mg_3Pd_5 we tend to classify it to be metastable.

In order to draw a comparison to the impact of iodine on the reaction between the two metals, reactions were also run without iodine. Mg and Pd powders were mixed in the molar ratio 1:2, pressed to pellets, and annealed at 600°C in evacuated fused silica tubes. After one week of heat treatment an X-ray powder diffractogram exclusively showed the broad reflections of AuCu-type $Mg_{0.9}Pd_{1.1}$ with $a = 4.273(3)$ and $c = 3.364(3)$ Å and Mg_xPd_{1-x} solid solution. According to the size of the lattice parameter $a = 3.901(2)$ Å, the solid solution is not yet saturated with Mg. This indicates that the reaction path might be similar to that of the iodine-catalyzed synthesis beginning with the

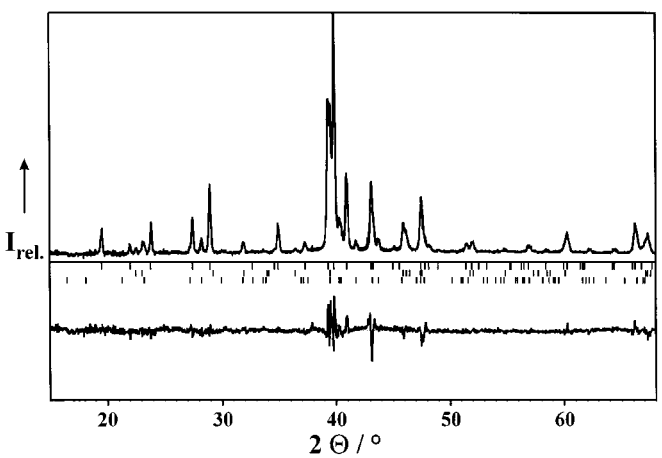

FIG. 6. Rietveld refinement of the 10-h sample containing Mg_3Pd_5 whose reflection positions are marked in the third line (first: $MgPd_2$, second: $MgPd_3$).

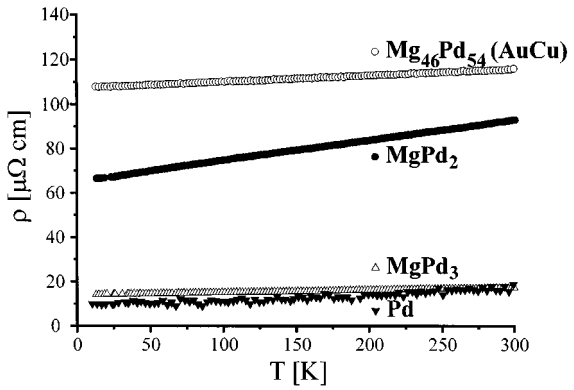

FIG. 7. Electrical resistivities of Pd, $MgPd_3$, $MgPd_2$, and $Mg_{46}Pd_{54}$.

formation of binary phases other than the final product (the AuCu-type phase had been found in the 0 h sample). The reaction is extremely slow under these conditions as after three months at 600°C the sample did not show yet any reflection of $MgPd_2$.

Measurements of the Electrical Resistivity

The palladium-rich phases in the Mg–Pd system all turned out to be very good electric conductors with resistivities, measured on pressed powder bars, ranging roughly from 10 to 120 μΩ cm (Fig. 7). For reasons of better comparability, the resistivity of elemental Pd as used for the synthesis also has been measured. Within the significance of the method, the conductivity of $MgPd_3$ is marginally smaller than that of Pd. With rising Mg content this feature is more distinct: at 300 K, the specific resistivities of $MgPd_2$ and $Mg_{46}Pd_{54}$ (AuCu structure) with $a = 4.2831(8)$, $c = 3.3883(9)$ Å exceed that of Pd by factors of approximately 5 and 7, respectively.

CONCLUSIONS

The iodine-promoted reaction of elemental magnesium and palladium provides access to the previously unknown ordered intermetallic phases $MgPd_2$, $MgPd_3$, and Mg_5Pd_3. The discovery of new binaries suggests catalytically stimulated reactions of elemental metals to be suitable for a rational synthesis of yet hidden, thermodynamically stable intermetallic phases.

Kinetic studies of the reaction between palladium and magnesium reveal that $MgPd_2$ is not formed directly but in a series of conproportion reactions following Ostwald's step rule. One of the intermediate phases is Mg_3Pd_5 which—by all indications—is thermodynamically metastable. It is the first example of a Ge_3Rh_5-type phase containing an alkaline earth metal.

ACKNOWLEDGMENTS

This work was financially supported by the Deutsche Forschungsgemeinschaft and the Fonds der Chemischen Industrie. A generous donation of palladium metal by Degussa-Hüls AG is gratefully acknowledged. We thank Christel Ruckert for the measurements of the electrical resistivities and Rüdiger Penzel for carrying out the DSC experiments.

REFERENCES

1. H.-F. Wu and L. Brewer, *J. Alloys Compd.* **247,** 1 (1997).
2. R. A. Alqasmi, S. Paasch, and H.-J. Schaller, *J. Alloys Compd.* **283,** 173 (1999).
3. S. V. Meschel and O. J. Kleppa, *J. Alloys Compd.* **297,** 162 (2000).
4. P. Villars and L. D. Calvert, "Pearson's Handbook of Crystallographic Data for Intermetallic Phases," 2nd ed. American Society for Metals, Metals Park, Ohio, 1996.
5. H.-B. Merker, H. Schäfer, and B. Krebs, *Z. Anorg. Allg. Chem.* **462,** 49 (1980).
6. M. Sauer, A. Engel, and H. Lueken, *J. Alloys Compd.* **183,** 281 (1992).
7. Ch. Wannek and B. Harbrecht, *Z. Anorg. Allg. Chem.* **626,** 1540 (2000).
8. R. Ferro, *J. Less-Common Met.* **1,** 424 (1959).
9. P. I. Kripyakevich and E. I. Gladyshevskii, *Kristallografiya* **5,** 577 (1960).
10. A. A. Nayeb-Hashemi and J. B. Clark, *Bull. Alloy Phase Diagrams* **6**(2), (1985).
11. E. M. Savitskii, V. F. Terekhova, and N. A. Birun, *Russ. J. Inorg. Chem.* **10,** 1228 (1962).
12. K. Yvon, W. Jeitschko, and E. Parthé, *J. Appl. Crystallogr.* **10,** 73 (1977).
13. V. Wagner and T. Degen, "DIFFRAKT: A Program for Processing X-Ray Powder Data." University of Bonn, 1992 to 1996.
14. Koninklijke Philips Electronics N.V., "X'Pert Plus, Version 1.0, Program for Crystallography and Rietveld Analysis." Almelo, NL, 1998–1999.
15. H. M. Rietveld, *J. Appl. Crystallogr.* **2,** 65 (1969).
16. G. M. Sheldrick, "SHELXS-86, Program for the Solution of Crystal Structures." University of Göttingen, Germany, 1985.
17. W. Jeitschko and R. O. Altmeyer, *Z. Naturforsch.* **45b,** 947 (1990).
18. Ch. Wannek and B. Harbrecht, *J. Alloys Compd.* **316,** 99 (2001).
19. G. A. Landrum, R. Hoffmann, J. Evers, and H. Boysen, *Inorg. Chem.* **37,** 5754 (1998).
20. U. Müller, "Anorganische Strukturchemie," Teubner Studienbücher Chemie, 2. Auflage, Stuttgart, 1992; U. Müller, "Inorganic Structural Chemistry." Wiley, New York, 1993.
21. E. Koch and W. Fischer, *Z. Kristallogr.* **211,** 215 (1996).
22. K. Schubert, S. Bhan, T. K. Biswas, K. Frank, and P. K. Panday, *Naturwiss.* **55,** 542 (1968).
23. K. Schubert, B. Kiefer, and M. Wilkens, *Z. Naturforsch.* **9a,** 987 (1954).
24. A. E. Carlsson and P. J. Meschter, Ab initio calculations, *in* "Intermetallic Compounds: Principles and Practice" (J. H. Westbrook and R. L. Fleischer, Eds.), Vol. 1, Chap. 3, p. 55. Wiley, Chichester, England, 1995.
25. H. Schäfer, "Chemische Transportreaktionen." Verlag Chemie, Weinheim, 1962; H. Schäfer, "Chemical Transport Reactions." New York, 1964.
26. R. Neddermann, R. Wartchow, and M. Binnewies, *Z. Anorg. Allg. Chem.* **624,** 733 (1998).

27. O. Bosholm, H. Oppermann, and S. Däbritz, *Z. Naturforsch.* **55b,** 614 (2000).
28. H. Schäfer and M. Trenkel, *Z. Anorg. Allg. Chem.* **414,** 137 (1975).
29. G. N. Papatheodorou, *J. Phys. Chem.* **77,** 472 (1973).
30. M. Binnewies, *Z. Anorg. Allg. Chem.* **435,** 156 (1977).
31. W. Lenhard, H. Schäfer, H.-U. Hürter, and B. Krebs, *Z. Anorg. Allg. Chem.* **482,** 19 (1981).